Two-dimensional titanium carbide (MXene) as surface-enhanced Raman scattering substrate

Asia Sarycheva[a], Taron Makaryan[a], Kathleen Maleski[a], Elumalai Satheeshkumar[b,c], Armen Melikyan[d], Hayk Minassian[e], Masahiro Yoshimura[b] and Yury Gogotsi[*a]

[a]Department of Materials Science and Engineering, and A.J. Drexel Nanomaterials Institute, Drexel University, Philadelphia, PA 19104, USA

[b]Promotion Center for Global Materials Research (PCGMR), Department of Material Science and Engineering, National Cheng Kung University, Tainan, Taiwan.

[c]Department of Chemistry, National Institute of Technology- Trichy, Tiruchirappalli – 620 015, Tamil Nadu, India.

[d]Russian-Armenian (Slavonic) State University, 0051, Yerevan, Armenia

[e]A. Alikhanian National Science Laboratory, 0036, Yerevan, Armenia

ABSTRACT: Noble metal (gold or silver) nanoparticles or patterned films are typically used as substrates for surface-enhanced Raman spectroscopy (SERS). Two-dimensional (2D) carbides and nitrides (MXenes) exhibit unique electronic and optical properties, including metallic conductivity and plasmon resonance in the visible or near-infrared range, making them promising candidates for a wide variety of applications. Herein, we show that 2D titanium carbide, $Ti_3C_2T_x$, enhances Raman signal from organic dyes on a substrate and in solution. As a proof of concept, MXene SERS substrates were manufactured by spray-coating and used to detect several common dyes, with calculated enhancement factors reaching ~10^6. Titanium carbide MXene demonstrates SERS effect in aqueous colloidal solutions, suggesting the potential for biomedical or environmental applications, where MXene can selectively enhance positively charged molecules.

Surface-enhanced Raman spectroscopy (SERS) is a promising technique for identification of small quantities of molecules due to its highly efficient, non-invasive and versatile nature.[1-7] Enhancement in Raman signal can be attributed to two general mechanisms, electromagnetic and chemical.[8] SERS substrates rely primarily on plasmonic effects in electromagnetic 'hot-spots' and highly concentrated charges originating from surface roughness.[9] The implementation of SERS is limited by the cost of SERS substrates (use of noble metals and expensive manufacturing), scalability and/or reproducibility (quantitative measurements require statistical data analysis[10]), and/or deposition of SERS particles exhibiting inhomogeneity on the substrate.[11] Defining and controlling the exact chemical mechanism (CM) of the SERS is even more elaborate due to complex processes involved during charge transfer, intra- and inter-band transitions, molecule adsorption and orientation versus the applied electromagnetic-field, and light absorption.[12] Nevertheless, to obtain a maximum enhancement factor (EF), it is desirable for a single system to benefit from both chemical and electromagnetic enhancement mechanisms.

Two-dimensional (2D) materials, such as N-doped graphene[13] and MoS_2, are capable of producing SERS depending on their electronic structure and various

chemical mechanisms.[14] Another family of 2D materials, transition metal carbides and nitrides (MXenes) display advantageous properties such as high metallic conductivity, hydrophilicity and flexibility. The most common MXene, $Ti_3C_2T_x$, where, T_x represents the surface terminations (-OH, -F, -O)[15], has already demonstrated promise in biosensing,[16-17] and other applications[18-20]. It has been calculated that the spatial position of the MXene functional groups can be critical for engineering materials with certain interband transitions and bandgaps.[21] $Ti_3C_2T_x$ has been demonstrated as a support for noble metal nanoparticles for their use in SERS[22], but the use of pristine MXene (such as $Ti_3C_2T_x$) materials as SERS substrates has not been previously reported.

Herein, we report on a method of producing $Ti_3C_2T_x$ SERS substrates with design-inherent hot-spots and CM-enabling electronic structure, yielding EF on the order of 10^5-10^6 as well as chemical selectivity to dye molecules. The spray-coating technique utilized in the present deposition method is versatile and scalable. We found an optimal percentage of surface coverage by performing a systematic study on a common dye, Rhodamine 6G (R6G). Additionally, to test the versatility of the system, other molecules with different absorption bands in the visible region were probed. We explored the effect of the laser wavelength and performed analytical and computational analysis for determining an enhancement mechanism. Even though TiC, TiN and other conductive bulk ceramics have been predicted to possess plasmonic properties,[23] there are no reports on the SERS effect from any MXene or a material in the Ti-C system in general.

The $Ti_3C_2T_x$ colloidal solution was prepared by the method reported previously.[24] A detailed description of the sample preparation (schematically illustrated in Figure 1a) is presented in Supporting Information (SI).

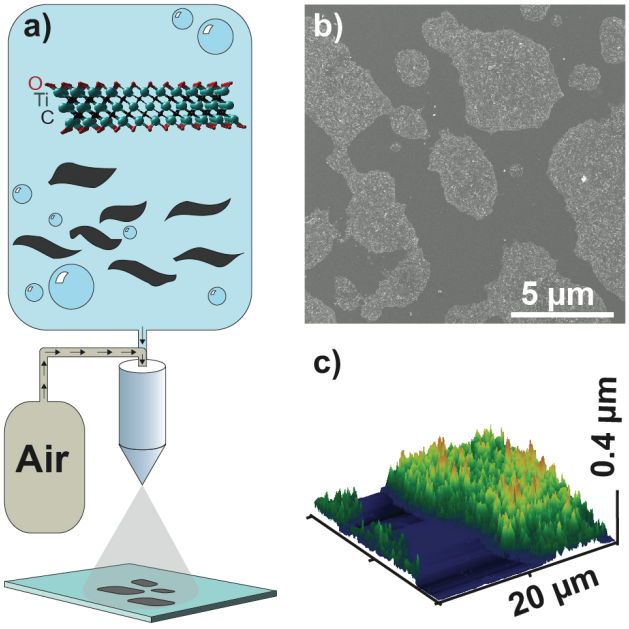

Figure 1. (a) Schematic describing fabrication and morphology of a $Ti_3C_2T_x$ SERS substrate; SEM (b) and AFM (c) images of $Ti_3C_2T_x$ on a glass substrate.

Briefly, the substrates for SERS analysis were prepared by air-gun spray-deposition of a colloidal solution of single- and few-layer $Ti_3C_2T_x$ flakes in water. Several coats on a silicon wafer were applied, with subsequent drying and dye deposition. The scanning electron microscope (SEM) image in Figure 1b shows the formation of MXene islands after 3 passes of spray-coating. Optical images in Figure S1 display the lateral expansion and eventual merging of the islands upon continued spraying. The layered structure of the spray-coated $Ti_3C_2T_x$ flakes can be observed in the SEM image in Figure S2. After depositing the dye molecules on the substrate, the edges of MXene islands were examined by atomic force microscopy (AFM) (Figure 1c). Further AFM analysis (Figure S5) confirms that the height of the islands reaches up to ~300 nm, exhibiting a root-mean square roughness of 69.2 nm.

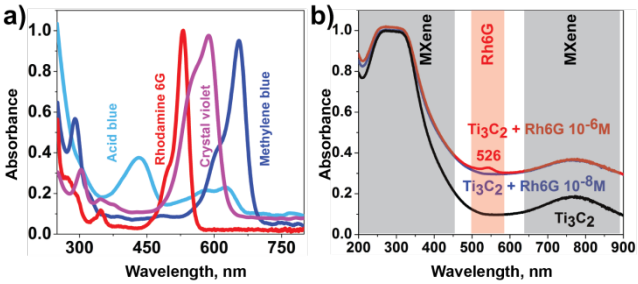

Figure 2: (a) UV-vis spectra of each dye used in this study; (b) UV-vis absorption spectra of pristine $Ti_3C_2T_x$ in aqueous solution and $Ti_3C_2T_x$ mixed with Rhodamine dye.

The UV-vis absorption spectra of R6G as well as other probed dyes such as methylene blue, acid blue, and crystal violet are presented in the Figure 2a. Due to the position of the R6G absorption peak, the 514 nm wavelength laser is selected to yield a high SERS signal as shown in Figure 3b. Mixing R6G at various concentrations in a water solution with MXene (presented in Figure 2b) reveals the spectrum of the dye notably starting from 10^{-6} M dye concentration (Figure 2b). Additionally, it should be noted that the absorption peaks of the MXene and the dye do not shift after mixing, indicating physisorption of the dye molecules on the MXene surface (in case of chemisorption, a peak shift would be evident). The UV-vis spectra of MXene films spray-coated with various thicknesses on glass have the absorption peak maximum around 750 nm (Figure S3 in SI). This explains the presence of the richer and more intense Raman peaks corresponding to enhancement of certain functional groups of the bare MXene films irradiated by different lasers (Figure S4 in SI). According to density-functional theory (DFT) computations,[25] the Raman peaks at 200 and 723 cm^{-1} are correspondingly attributed to the Ti-C and C-C vibrations (A_{1g} symmetry) of the oxygen-terminated $Ti_3C_2O_2$. The peak at 620 cm^{-1} comes mostly from E_g vibrations of the C atoms in the OH-terminated MXene.

The peaks at 389 and 580 cm^{-1} are attributed to the O atoms E_g and A_{1g} vibrations, respectively. The 282 and 519 cm^{-1} (the latter is enhanced when using a 788 nm excitation) are occurring due to the contribution of H atoms in the OH groups of $Ti_3C_2T_x$.

Distinct R6G peaks can be spotted in Figure 3a in the case of 10^{-6} M solution drop-casted on the MXene substrate produced by 3 spray-coating passes. At 10^{-7} M dye concentration, the most intense vibrational peaks of R6G are still detectable suggesting the $Ti_3C_2T_x$ substrates promote a high enhancement factor, even at low concentrations of dye. Enhancement of Raman scattering due to charge transfer absorption was observed for TiO_2 nanoparticles[26], which chemically resemble the surface of MXenes. However, all our experiments were conducted on freshly prepared MXene samples and no traces of TiO_2 were observed by Raman spectroscopy. To study the dependence of the SERS performance on the quality of $Ti_3C_2T_x$ deposition (Figure 3b), we drop-casted the same concentration of R6G molecules on Si/SiO_2 substrates with $Ti_3C_2T_x$ spray-coated after 3, 10 and 20 passes. The substrate spray-coated 3 times exhibited a higher EF than those with thicker and more uniform coatings (a larger number of spray-deposition passes). The relationship between the SERS performance and the quality of the $Ti_3C_2T_x$ substrates shows the significance of the 'hot-spot' effect in the electromagnetic mechanism. In Figure 3c, the SERS peaks of the 10^{-6} M drop-casted R6G on the $Ti_3C_2T_x$ islands are excited by 488 and 514 nm lasers in comparison. Evidently, certain peaks (~1528 cm^{-1} and ~1575 cm^{-1}) are enhanced stronger by the 514 nm excitation than by the 488 nm laser, which supports the interband transition/charge transfer mechanism of the enhancement. Additionally, the 10^{-6} M R6G concentration can be detected in a 1 mg/mL aqueous solution of $Ti_3C_2T_x$ with both 488 and 514 nm lasers (Figure 3c). The SERS spectrum acquired with the 488 nm excitation has a stronger fluorescence background and less prominent peaks of the dye as compared to that of the 514 nm laser, possibly due to using an excitation which was shifted to a higher energy than the absorption peak (Figure 2a). Finally, calculating the SERS enhancement of R6G from the data in Figure 3d (see SI, Section 2), we get the factors of ~1.2×10^6 and 5.3×10^5, for the 488 and 514 nm lasers, respectively.

To assess the distribution of the 10^{-6} M concentrated R6G molecules on the surface of the MXene islands formed after 3 passes of spray-coating on the Si/SiO_2 substrate, we performed a 514 nm excitation Raman intensity mapping (normalized false rainbow-color coded images in Figure 3e-f). Figure 3e reveals a thicker coverage (more flakes, hence a more uniform and flat surface, and consequently fewer hot-spots) of the substrate by MXene on the left side of the mapped area (Figure 3e). The intensity of the sum of the two peaks (614 and 776 cm^{-1}) of the R6G from the SERS is higher at the edges of the MXene island (Figure 3f) confirming the contribution of 'hot-spots' to the Raman signal enhancement. These observations are consistent with the optical image of the same area (Figure 3g), and with the analysis of Figure 3b.

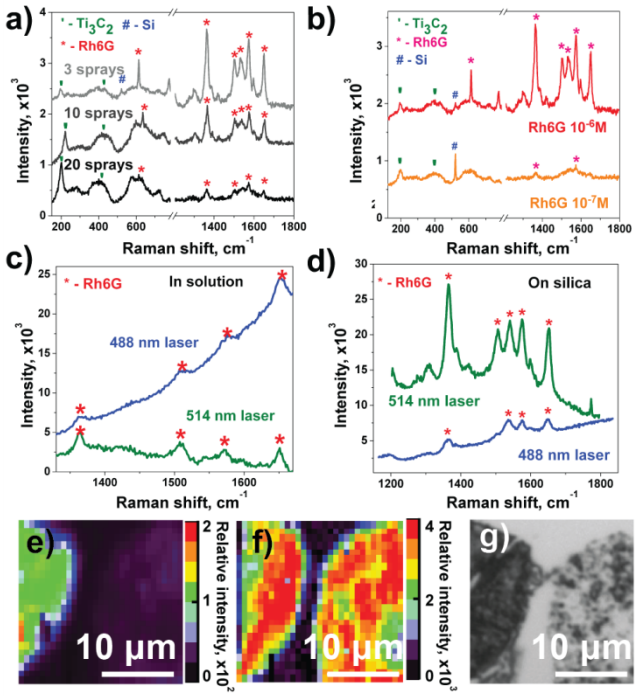

Figure 3: (a) SERS enhancement (514 nm excitation) of Rhodamine 6G on $Ti_3C_2T_x$ MXene substrates of different thickness (number of spray-coating passes); (b) SERS effect of various R6G concentrations drop-casted on MXene/SiO_2/Si substrate (3 passes of MXene spray-coating, 514 nm); Enhancement using 488 and 514 nm lasers in an aqueous colloidal solution (c) and on a MXene/SiO_2/Si substrate (3 passes) (d); Raman mapping of the interstitial area of the same substrate, with color-coding of the intensity of the sum of (e) $Ti_3C_2T_x$ MXene peaks, and (f) R6G peaks (drop-casted on MXene from a 10^{-6} M solution). An optical image of the Raman mapped area (g).

As a proof-of-concept, SERS performance was probed with other dyes besides R6G, including methylene blue (MB), crystal violet (CV) and acid blue (AB). Corresponding to the position of their absorption peaks, MB and CV were excited through the 633 nm laser and AB through the 514 nm laser (Figure 4). A higher SERS EF from MB molecules (Figure 4a) is expected compared to R6G, due to the high UV-vis absorption of MB (peak at 680 nm) near 633 nm region as well as being close to the absorption peak of $Ti_3C_2T_x$ (Figure 2b). Indeed, we obtained a EF value of 1.6×10^6 for MB and in comparison, the CV dye (Figure 4b) having an absorption peak at 588 nm, exhibits an EF of 5×10^5.

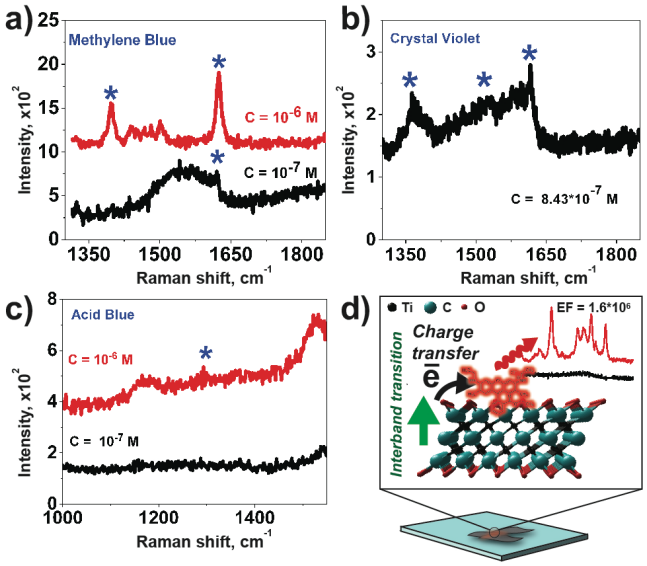

Figure 4: SERS spectra of other dyes used in this study: methylene blue (a), crystal violet (b), and acid blue (c). SERS mechanism. Hot spots (surface roughness, red) are causing field enhancement. Interband transitions in MXene flakes induce strong polarization supporting SERS, and also enhancing subsequent charge transfer to the dye molecule (d).

Furthermore, AB dye (Figure 4c) provides a significantly lower SERS EF (2.7×10^3) despite having absorption bands between 400 and 650 nm (Figure 2b). This could be explained by the charge of the dye. MB is cationic in nature, suggesting it may display good adsorption on the negatively charged $Ti_3C_2T_x$ surface, however AB is anionic, indicating molecules may not adsorb onto the $Ti_3C_2T_x$ surface, as demonstrated before.[27] This finding, which highlights the importance of charge transfer to the dye for the enhancement, suggests that a selective SERS may be achieved in solution where molecules are preferentially adsorbed on the MXene surface.

To further support the experimental analysis, Figures S6 and S7 show the absorption spectra of $Ti_3C_2T_x$ flakes with various lateral sizes calculated by an analytical and a finite element method respectively, using dielectric function of a $Ti_3C_2T_x$ film.[28] For the transversal polarization case, the first absorption peak is calculated to be in the 500-700 nm range (centered at ~620 nm). As for the longitudinal incidence, it possesses the first absorption peak in the 700-800 nm range (centered at ~780 nm). Since, for both polarizations, those peaks remain the same for large aspect ratio (300 and 500 nm in diameter) MXene flakes, we state that the nature of the first peak is interband transitions. The second peak of the longitudinal oscillations in the near-infrared is highly dependent on the geometry, which is typical for surface plasmons. The high amplitude of this longitudinal plasmonic band could have contributed to a red-shifted interband transition peak, as compared to the transversal one. Considering all the observations and discussions above, we depict the possible mechanism by hypothesizing that the SERS occurs at 'hot-spots' due to an interband transition to the vacant energy states of the functional groups of MXene,[21] followed by a charge transfer to the adsorbed molecule. Subsequently, a relaxation causes emission of photons detected as Raman scattering (Figure 4b). It is, however, necessary to conduct a deeper study for determining the exact enhancement mechanisms of $Ti_3C_2T_x$ MXene.

We have demonstrated a large (10^6) Raman signal enhancement of organic dyes on the surface of 2D $Ti_3C_2T_x$ MXene, with detection of Rhodamine 6G at 10^{-7} M concentration. Moreover, a simple, cost-effective air-gun, spray-coating method was developed for fabricating SERS substrates without noble metals and thin $Ti_3C_2T_x$ islands with rough surfaces and edges. Synergy between electromagnetic and chemical enhancements of $Ti_3C_2T_x$ SERS substrates displays the potential of using this material for bio-chemical molecular sensing or SERS sensors. Moreover, being mindful that $Ti_3C_2T_x$ is just one material in a family of ~20 MXenes produced and millions of compositions possible (if solid solutions are taken into account),[29] there are many reasons to think that further improvement and optimization is possible through fine control of material deposition, nanofabricated patterns, or control/tunability of material properties.

ASSOCIATED CONTENT

Supporting Information

The supporting information is available free of charge on the ACS publications website at DOI:

Experimental preparations, SERS EF calculations, sample characterization (Raman, UV-vis, AFM), absorption calculations.

AUTHOR INFORMATION

Corresponding Author:

*Y.G. : gogotsi@drexel.edu

Notes:

The authors declare no competing financial interest.

ACKNOWLEDGMENTS

This work was funded by the Fluid Interface Reactions, Structures and Transport (FIRST) Center, an Energy Frontier Research Center funded by the U.S. Department of Energy, Office of Science, Office of Basic Energy Sciences. The authors are grateful to the Centralized Research Facilities (CRF) of the Drexel University for access to SEM. We also thank Tyler Mathis for help with SEM imaging and Tomas Polakovic for AFM (Drexel University).

REFERENCES

(1) Camden, J. P.; Dieringer, J. A.; Wang, Y.; Masiello, D. J.; Marks, L. D.; Schatz, G. C.; Van Duyne, R. P. *JACS* **2008,** *130*, 12616-12617.

(2) Kneipp, K.; Wang, Y.; Kneipp, H.; Perelman, L. T.; Itzkan, I.; Dasari, R.; Feld, M. S. *Phys Rev Lett* **1997,** *78*, 1667-1670.

(3) Lee, S. J.; Guan, Z. Q.; Xu, H. X.; Moskovits, M. *J Phys Chem C* **2007,** *111*, 17985-17988.

(4) Jaworska, A.; Fornasaro, S.; Sergo, V.; Bonifacio, A. *Biosensors (Basel)* **2016,** *6*, 47.
(5) Kneipp, J. *ACS Nano* **2017,** *11*, 1136-1141.
(6) Vitol, E. A.; Friedman, G.; Gogotsi, Y. *J. Nanosci. Nanotechnol.* **2014,** *14*, 3046-51.
(7) Gao, Y.; Longenbach, T.; Vitol, E. A.; Orynbayeva, Z.; Friedman, G.; Gogotsi, Y. *Nanomedicine (London)* **2014,** *9*, 153-68.
(8) Schlücker, *S. Angew. Chem. Int. Ed.* **2014,** 53, 4756-4795.
(9) Radziuk, D.; Moehwald, H. *PCCP* **2015,** *17*, 21072-21093.
(10) Vitol, E. A.; Friedman, G.; Gogotsi, Y. *J. Nanosci. Nanotechnol.* **2014,** *14*, 3046-3051.
(11) Sharma, B.; Fernanda Cardinal, M.; Kleinman, S. L.; Greeneltch, N. G.; Frontiera, R. R.; Blaber, M. G.; Schatz, G. C.; Van Duyne, R. P. *MRS Bulletin* **2013,** *38*, 615-624.
(12) Aikens, C. M.; Madison, L. R.; Schatz, G. C. *Nat Photon* **2013,** *7*, 508-510.
(13) Feng, S.; dos Santos, M. C.; Carvalho, B. R.; Lv, R.; Li, Q.; Fujisawa, K.; Elías, A. L.; Lei, Y.; Perea-López, N.; Endo, M.; Pan, M.; Pimenta, M. A.; Terrones, M. *Sci. Advan* **2016,** *2*, e1600322.
(14) Ling, X.; Fang, W.; Lee, Y. H.; Araujo, P. T.; Zhang, X.; Rodriguez-Nieva, J. F.; Lin, Y.; Zhang, J.; Kong, J.; Dresselhaus, M. S. *Nano Lett* **2014,** *14*, 3033-40.
(15) Hope, M. A.; Forse, A. C.; Griffith, K. J.; Lukatskaya, M. R.; Ghidiu, M.; Gogotsi, Y.; Grey, C. P. *PCCP* **2016,** *18*, 5099-102.
(16) Rakhi, R. B.; Nayak, P.; Xia, C.; Alshareef, H. N., Novel. *Sci Rep* **2016,** *6*, 36422.
(17) Rasool, K.; Helal, M.; Ali, A.; Ren, C. E.; Gogotsi, Y.; Mahmoud, K. A. *ACS Nano* **2016,** *10*, 3674-84.
(18) Ren, C. E.; Hatzell, K. B.; Alhabeb, M.; Ling, Z.; Mahmoud, K. A.; Gogotsi, Y. *J. Phys. Chem. Lett.* **2015,** *6*, 4026-31.
(19) Shahzad, F.; Alhabeb, M.; Hatter, C. B.; Anasori, B.; Man Hong, S.; Koo, C. M.; Gogotsi, Y. *Science (New York, N.Y.)* **2016,** *353*, 1137-40.
(20) Anasori, B.; Lukatskaya, M. R.; Gogotsi, Y. *Nat Rev Mat* **2017,** *2*, 16098.
(21) Magne, D.; Mauchamp, V.; Celerier, S.; Chartier, P.; Cabioc'h, T. *Phys Rev B* **2015,** *91*,201409
(22) Satheeshkumar, E.; Makaryan, T.; Melikyan, A.; Minassian, H.; Gogotsi, Y.; Yoshimura, M. *Scientific Reports* **2016,** *6*, 32049.
(23) Kumar, M.; Umezawa, N.; Ishii, S.; Nagao, T. *ACS Photon* **2016,** *3*, 43-50.
(24) Lipatov, A.; Alhabeb, M.; Lukatskaya, M. R.; Boson, A.; Gogotsi, Y.; Sinitskii, A. *Adv Electron Mater* **2016,** *2*, 1600255.
(25) Hu, T.; Wang, J.; Zhang, H.; Li, Z.; Hu, M.; Wang, X. *PCCP* **2015,** *17*, 9997-10003.
(26) Yang, L., Jiang, X., Ruan, W., Zhao, B., Xu, W., & Lombardi, *J Raman Spectrosc* **2009** *40*, 2004-2008.
(27) Mashtalir, O.; Cook, K. M.; Mochalin, V. N.; Crowe, M.; Barsoum, M. W.; Gogotsi, Y. *J Mater Chem A* **2014,** *2*, 14334-14338.
(28) Dillon, A. D.; Ghidiu, M. J.; Krick, A. L.; Griggs, J.; May, S. J.; Gogotsi, Y.; Barsoum, M. W.; Fafarman, A. T., Highly. *Adv Func Mater* **2016,** *26*, 4162-4168.
(29) Tan, T. L.; Jin, H. M.; Sullivan, M. B.; Anasori, B.; Gogotsi, Y. *ACS Nano* **2017**, 11, 4407-4418